

Prospects for detecting the dark matter particles and primordial black holes with the Hongmeng mission using the 21 cm global spectrum at cosmic dawn

Meng-Lin Zhao, ^{a,b} Sai Wang, ^{b,*} Xin Zhang ^{a,c,d,*}

^aLiaoning Key Laboratory of Cosmology and Astrophysics, College of Sciences, Northeastern University, Shenyang 110819, China

^bTheoretical Physics Division, Institute of High Energy Physics, Chinese Academy of Sciences, Beijing 100049, China

^cNational Frontiers Science Center for Industrial Intelligence and Systems Optimization, Northeastern University, Shenyang 110819, China

^dMOE Key Laboratory of Data Analytics and Optimization for Smart Industry, Northeastern University, Shenyang 110819, China

E-mail: mlzhao@stu.neu.edu.cn, wangsai@ihep.ac.cn, zhangxin@mail.neu.edu.cn

Abstract. Dark matter is believed to account for a significant portion of the mass in the universe, exerting a critical influence on the formation and evolution of cosmic structures. This research delves into the processes of annihilation and decay of dark matter particles, which generate observable signals that deepen our comprehension of their characteristics and behaviors. Furthermore, the study explores the potential role of primordial black holes, with a focus on the emissions of Hawking radiation that could offer valuable insights into their distribution and size range. A key aspect of this investigation revolves around the 21 cm signal, a vital tool for scrutinizing the effects of dark matter particles and primordial black hole phenomena on the intergalactic medium. The upcoming Hongmeng mission, featuring a lunar orbital interferometer array, is poised to revolutionize our ability to observe the 21 cm signal. By conducting measurements devoid of atmospheric disturbances, the mission will significantly boost sensitivity to subtle signals associated with dark matter particle annihilation, decay, and primordial black hole emissions. This study assesses the expected performance of the Hongmeng mission in detecting these telltale signs and aims to unveil fresh insights into the nature and interactions of dark matter particles and primordial black hole emissions through a meticulous analysis of the global 21 cm spectrum. The mission holds immense promise for reshaping our understanding of the universe's concealed components.

*Corresponding author.

Contents

1	Introduction	1
2	Scenarios of exotic energy	3
2.1	Annihilation and decay of DM particles	3
2.2	Hawking radiation of PBHs	3
3	Influence of exotic energy on the 21 cm global signal	4
4	Fisher-matrix forecasting	5
5	Hongmeng’s discovering potential	7
5.1	Results for DM particles	7
5.2	Results for PBHs	11
6	Summary	13

1 Introduction

The concept of dark matter (DM) is postulated to account for a significant portion of the universe’s mass, as evidenced by observations of galactic rotations, galaxy cluster dynamics, gravitational lensing, the anisotropies in the cosmic microwave background (CMB), and other phenomena, with recent reviews in Refs. [1–9] and references therein. Despite being invisible, the gravitational influence of DM plays a crucial role in the formation and evolution of cosmic structures. As a result, a variety of candidate models for DM have been proposed in the scientific literature, with reviews available in Refs. [6, 7, 10] and references therein. These candidate models can generally be classified into three categories: particles, macroscopic objects, and modifications to gravity, each encompassing a diverse array of theoretical frameworks. In this study, our focus is primarily on the former two categories.

The annihilation and decay of DM particles are pivotal processes within the domain of DM research (see reviews in Refs. [11–19] and references therein). On the one hand, DM annihilation occurs when two DM particles collide, resulting in the conversion into other particles and the potential generation of detectable signals such as gamma rays or cosmic rays. These signals offer valuable insights into the interactions among DM particles. On the other hand, DM decay involves the spontaneous conversion of a DM particle into lighter particles, providing essential information regarding the stability and lifetime of DM particles. Investigations into these processes are crucial for advancing our understanding of DM and present unique opportunities to probe the nature of DM through astronomical observations.

Should primordial black holes (PBHs) constitute a significant portion of DM, the observation and analysis of their Hawking radiation emissions hold promise for shedding light on their fundamental characteristics, e.g., their abundance as a function of their masses. The theoretical framework of Hawking radiation, as proposed by Stephen Hawking [20], posits that black holes can emit radiation and particles such as gamma rays, cosmic rays or neutrinos, due to quantum effects near the event horizon. Through the meticulous study of this radiation, we can not only deepen our understanding of PBHs as viable DM candidates, but

also find potential implications for the nature of quantum gravity. Relevant constraints on the PBH mass function are shown in Refs. [21–25] and references therein.

The 21 cm signal plays a pivotal role as an essential tool in the study of DM. Processes involving DM particle annihilation and decay, as well as PBH Hawking radiation emissions, can introduce exotic energy into the intergalactic medium (IGM) [26–28], leading to significant alterations in the thermal and ionization histories of the universe. These modifications impact the spin temperature of neutral hydrogen, thereby influencing the 21 cm brightness temperature, which is closely tied to this spin temperature. The importance of the 21 cm signal in unraveling the mysteries of DM is underscored by these connections. Notably, compared to other cosmological probes such as the CMB [13, 29–31] and Lyman- α forest [32], the 21 cm absorption lines demonstrate heightened sensitivity to phenomena occurring during the era of cosmic dawn with redshifts $z \sim 10 - 20$. In particular, the Experiment To Detect The Global EoR Signature (EDGES) reported an absorption feature of 21 cm global signal at $z \simeq 17$ [33]. Analyzing this signal, researchers placed upper limits on parameters characterizing the DM particle annihilation and decay [28] as well as the PBH mass function [34, 35]. However, such a signal was recently rejected by the Spectrograph For The arecibo Radar And Radiation Astronomy (SARAS 3) at 95.3% confidence level [36].

Looking ahead, the Hongmeng mission [37] offers a vast of advantages for conducting observations of the 21 cm signal. With ten satellites to weave a lunar orbital interferometer array, it is capable of fulfilling the full-sky detection in the frequency bands from 0.1 MHz to 120 MHz. It also benefits from a vantage point that is free from the atmospheric interference and light pollution that can hinder ground-based observations. This allows for clearer and more precise measurements of cosmic phenomena, providing valuable insights into the properties of the IGM. The stability and controlled environment of lunar orbit also enable the Hongmeng mission to conduct long-term observations with enhanced consistency and accuracy, facilitating the detection of subtle signals and anomalies in the 21 cm signal. In addition, the lunar orbital satellite array can leverage the Moon’s gravitational influence to optimize its trajectory and positioning, maximizing the efficiency and coverage of its observations. By capitalizing on these advantages, the Hongmeng mission is expected to make significant contributions to understanding the nature of exotic energy sources such as DM particles and PBHs in principle.

In this work, we study the prospective sensitivity of the Hongmeng mission to detect the annihilation and decay of DM particles, as well as the Hawking radiation emissions of PBHs. By leveraging the advanced capabilities of the Hongmeng lunar orbital satellite array, we aim to probe the interactions of DM particles and the potential signatures of PBHs within the cosmic landscape. The unique positioning of the Hongmeng mission in lunar orbit offers unparalleled advantages for observing subtle signals associated with DM annihilation, decay processes, and PBH emissions, providing a new perspective on these elusive cosmic entities. Through detailed analyses of the 21 cm global spectrum collected by the Hongmeng mission, we seek to uncover clues about the nature, properties, and interactions of DM particles and PBHs, shedding light on fundamental questions in astrophysics and cosmology. This innovative approach holds the potential to revolutionize our understanding of the universe’s hidden sector.

The subsequent sections of this paper are structured as follows. Section 2 presents the scenarios of exotic energy injection considered in this study, with a summary of their effects on the IGM and 21 cm global signal outlined in Section 3. Section 4 elaborates on the Fisher information matrix and parameter settings employed, while Section 5 showcases the primary

findings. Finally, Section 6 offers a concise discussion and summary of the study’s outcomes. In our present study, we adhere to the cosmological parameters outlined in the Planck 2018 results [38], specifically utilizing $(\Omega_m, \Omega_b, \Omega_\Lambda, h, \sigma_8, n_s) = (0.31, 0.049, 0.69, 0.68, 0.81, 0.97)$. Here, the first three parameters represent the present-day energy-density fractions of non-relativistic matter, baryons, and dark energy, while the latter three correspond to the dimensionless Hubble constant, the amplitude of matter fluctuations, and the spectral index of primordial curvature perturbations. Throughout this work, the speed of light is denoted as c , and the Boltzmann constant is k_B .

2 Scenarios of exotic energy

In this section, we briefly summarize the formulas for scenarios of exotic energy considered in our present work. The present-day energy density of DM is represented as $\rho_{\text{DM}} = \rho_c \Omega_{\text{DM}}$, where we have $\Omega_{\text{DM}} = \Omega_m - \Omega_b$, and ρ_c is a critical energy density of the present-day cosmos.

2.1 Annihilation and decay of DM particles

The annihilation and decay of DM particles can give rise to particles of the standard model, including primary and secondary products. Three classes of primary particles are considered: photons, electron-positron pairs, and bottom-anti-bottom quark pairs. Secondary particles, such as photons, electrons, protons, neutrinos, and others, are generated from primary particles through processes such as annihilation, decay, and hadronization [39]. To model these processes, we employ the PPPC4DMID [40] and `pythia` [41] simulations. In the following section, we focus solely on photons, electrons, and positrons as they are effective in depositing energy into the IGM [42, 43].

We consider an s-wave annihilation channel of DM particles, regardless of the primary products. The exotic energy injected into the IGM gas per unit volume per unit time is given by [44]

$$\left(\frac{dE}{dVdt} \right)_{\text{inj,ann}} = \rho_{\text{DM}}^2 \mathcal{B}(z) (1+z)^6 c^2 \frac{\langle \sigma v \rangle}{m_\chi}, \quad (2.1)$$

where $\mathcal{B}(z)$ stands for a booster factor due to clumping of DM, as comprehensively investigated in Ref. [45], z is cosmological redshift, $\langle \sigma v \rangle$ denotes the thermally-averaged annihilation cross-section of DM particles, and m_χ is the mass of DM particles. Here, we assume the fraction of DM particles which can annihilate to be unity, i.e., $f_{\text{ann}} = 1$. Otherwise, we should multiply a factor of f_{ann}^2 at the right hand side of the above formula.

For a decay channel of DM particles, regardless of primary products, we get the exotic energy injected into IGM gas per unit volume per unit time of the form [44]

$$\left(\frac{dE}{dVdt} \right)_{\text{inj,dec}} = \rho_{\text{DM}} (1+z)^3 c^2 \frac{1}{\tau}, \quad (2.2)$$

where τ stands for a lifetime of DM particles. Here, we assume the fraction of DM particles which can decay to be unity, i.e., $f_{\text{dec}} = 1$. Otherwise, we should multiply a factor of f_{dec} at the right hand side of the above formula.

2.2 Hawking radiation of PBHs

The Hawking radiation of PBHs can emit particles of the standard model [20]. We adopt the `BlackHawk` [46] to obtain the particle spectra, denoted as $d^2N/(dEdt)$. When considering

PBHs in a mass range of $M_{\text{PBH}} \sim 10^{15} - 10^{18}$ g, we focus on photons and electron-positron pairs as emission products. Therefore, the exotic energy injected into IGM gas per unit volume per unit time is given by [34, 39, 44, 47]

$$\left(\frac{dE}{dVdt} \right)_{\text{inj, PBH}} = \int_0^{5\text{GeV}} \left. \frac{d^2N}{dEdt} \right|_{\gamma} n_{\text{PBH}} E dE + \int_{m_e c^2}^{5\text{GeV}} \left. \frac{d^2N}{dEdt} \right|_{e^\pm} n_{\text{PBH}} (E - m_e c^2) dE, \quad (2.3)$$

where the first and second terms at the right hand side stand for contributions from photons and electron-positron pairs, respectively. Here, m_e is the mass of electrons. n_{PBH} denotes the comoving number density of PBHs, represented as [48, 49]

$$n_{\text{PBH}} = \frac{f_{\text{PBH}} \rho_{\text{DM}}}{M_{\text{PBH}}}, \quad (2.4)$$

where f_{PBH} is the abundance of PBHs as DM. In this work, we assume a monochromatic mass function of PBHs for the sake of illustration. Nevertheless, our research can be straightforwardly extended to study other mass functions of PBHs if necessary.

3 Influence of exotic energy on the 21 cm global signal

Considering the exotic energy injection and deposition efficiency, we study influence of the exotic energy on the thermal and ionization histories of the IGM gas. Eventually, we demonstrate changes of the 21 cm global spectrum at cosmic dawn.

The differential 21 cm brightness temperature for the 21 cm global signal is defined as [50, 51]

$$T_{21}(z) = 23 x_{\text{HI}}(z) \left(\frac{0.15}{\Omega_{\text{m}}} \right)^{\frac{1}{2}} \left(\frac{\Omega_{\text{b}} h^2}{0.02} \right) \left(\frac{1+z}{10} \right)^{\frac{1}{2}} \left[1 - \frac{T_{\text{CMB}}(z)}{T_{\text{S}}(z)} \right] \text{ mK}, \quad (3.1)$$

where x_{HI} stands for the neutral fraction of hydrogen, T_{CMB} is a temperature of CMB radiation at z , and T_{S} denotes a spin temperature of hydrogen at z . Defined as a ratio between the populations of triplets and singlet of neutral hydrogen, the spin temperature is [51]

$$T_{\text{S}}^{-1} = \frac{T_{\text{CMB}}^{-1} + x_{\alpha} T_{\alpha}^{-1} + x_{\text{c}} T_{\text{k}}^{-1}}{1 + x_{\alpha} + x_{\text{c}}}, \quad (3.2)$$

where T_{α} stands for a color temperature of the Lyman- α photons, x_{α} is a Lyman- α coupling coefficient due to resonant scattering, i.e., the Wouthuysen-Field effect [47, 50], T_{k} denotes a kinetic temperature of the IGM gas, and x_{c} is a coupling coefficient due to collisions between two hydrogen atoms, hydrogen atoms and electrons, as well as hydrogen atoms and protons [50, 51]. Due to frequent scattering, the color temperature is tightly coupled to the kinetic temperature, i.e., $T_{\alpha} \simeq T_{\text{k}}$. The exotic energy injection can change the evolution histories of x_{HI} , T_{k} , and x_{α} , leading to changes of the 21 cm global signal.

Firstly, the evolution of x_{e} (i.e., the ionization fraction $x_{\text{e}} = 1 - x_{\text{HI}}$) and T_{k} is ruled by the following system of equations [47, 48, 50, 51]

$$\frac{dx_{\text{e}}}{dz} = \frac{dt}{dz} (\Lambda_{\text{ion}}^{\text{exo}} + \Lambda_{\text{ion}}^{\text{X}} + \alpha_{\text{A}} C x_{\text{e}}^2 n_{\text{H}}), \quad (3.3)$$

$$\frac{dT_{\text{k}}}{dz} = \frac{2}{3k_{\text{B}}(1+x_{\text{e}})} \frac{dt}{dz} (\epsilon_{\text{heat}}^{\text{exo}} + \epsilon_{\text{heat}}^{\text{X}} + \epsilon_{\text{heat}}^{\text{IC}}) + \frac{2T_{\text{k}}}{3n_{\text{b}}} \frac{dn_{\text{b}}}{dz} - \frac{T_{\text{k}}}{1+x_{\text{e}}} \frac{dx_{\text{e}}}{dz}. \quad (3.4)$$

Here, we introduce $dt/dz = 1/[H(z)(1+z)]$ with t and $H(z)$, respectively, being the cosmic time and Hubble parameter at z . α_A stands for the case-A recombination coefficient. C is the clumping factor. n_H and n_b , respectively, denotes the number densities of hydrogen and baryons. The ionizing rate per baryon due to astrophysical X rays is denoted as Λ_{ion}^X . The heating rates per baryon due to astrophysical X rays and inverse-Compton scattering are denoted as ϵ_{heat}^X and $\epsilon_{\text{heat}}^{\text{IC}}$, respectively. The above astrophysical processes can be simulated with 21cmFAST [52], and the above equations can also be solved with the same package.

Regarding contributions of the exotic energy injection, the ionizing and heating rates per baryons, respectively, can be represented as [47, 48]

$$\Lambda_{\text{ion}}^{\text{exo}} = F_{\text{HI}}(z) \frac{1}{n_b} \frac{n_H}{n_b} \frac{1}{E_{\text{ion}}^{\text{HI}}} \left(\frac{dE}{dVdt} \right)_{\text{inj,L}} + F_{\text{He}}(z) \frac{1}{n_b} \frac{n_{\text{He}}}{n_b} \frac{1}{E_{\text{ion}}^{\text{He}}} \left(\frac{dE}{dVdt} \right)_{\text{inj,L}}, \quad (3.5)$$

$$\epsilon_{\text{heat}}^{\text{exo}} = F_{\text{heat}}(z) \frac{1}{n_b} \left(\frac{dE}{dVdt} \right)_{\text{inj,L}}. \quad (3.6)$$

Here, a subscript L stands for annihilation, decay, and Hawking radiation, respectively. n_{He} is the number density of helium. $E_{\text{ion}}^{\text{HI}}$ and $E_{\text{ion}}^{\text{He}}$ denote the ionization energies of hydrogen and helium, respectively. In addition, F_{HI} , F_{He} , and F_{heat} stand for the energy deposition efficiencies through processes of hydrogen ionization, helium ionization, and heating, respectively. They can be calculated with DarkHistory [44].

Secondly, the Lyman- α coupling coefficient depends on the total flux of Lyman- α photons, i.e., [47]

$$x_\alpha = \frac{1.7 \times 10^{11}}{1+z} S_\alpha (J_\alpha^{\text{exo}} + J_\alpha^X + J_\alpha^*), \quad (3.7)$$

where S_α is a quantum mechanical correction [50], J_α^X and J_α^* , respectively, stand for the fluxes of Lyman- α photons from astrophysical X rays and stellar emissions, with detailed calculations with 21cmFAST [52]. Here, a contribution from the exotic energy injection is given by [48]

$$J_\alpha^{\text{exo}} = F_{\text{exc}}(z) \frac{1}{n_b} \frac{cn_b}{4\pi} \frac{1}{E_\alpha} \frac{1}{H(z)\nu_\alpha} \left(\frac{dE}{dVdt} \right)_{\text{inj,L}}, \quad (3.8)$$

where F_{exc} stands for the energy deposition efficiency through process of hydrogen excitation, with detailed calculations with DarkHistory [44], E_α denotes the Lyman- α energy, and ν_α is the Lyman- α frequency.

4 Fisher-matrix forecasting

To study the sensitivity of the Hongmeng mission to search for DM particles and PBHs, we adopt the Fisher information matrix, which is particularly useful for theoretical analysis.

Let us to begin with the to-some-extent general form of Fisher information matrix [53]

$$F_{ij} = \frac{1}{2} \text{Tr} [C^{-1} C_{,i} C^{-1} C_{,j} + C^{-1} (\mu_{,i} \mu_{,j}^T + \mu_{,j} \mu_{,i}^T)], \quad (4.1)$$

where C stands for a covariance matrix of data, $C_{,i}$ denotes a derivative to the i -th parameter, denoted as p_i , and μ is the expectation value of an observable. The observable for 21 cm global experiments is the antenna temperature T_{sky} in a frequency band ν , represented as [47, 54, 55]

$$T_{\text{sky}}(\nu) = T_{\text{fg}}(\nu) + T_{21}(\nu), \quad (4.2)$$

where T_{fg} and T_{21} , respectively, stand for the foreground temperature and differential 21 cm brightness temperature. Practically, we use a power-law to characterize the foreground temperature, i.e., [37, 56]

$$T_{\text{fg}}(\nu) = 16.3 \times 10^6 \text{ K} \left(\frac{\nu}{2 \text{ MHz}} \right)^{-2.53}. \quad (4.3)$$

The covariance is diagonal, since the detection in different frequency bands, labeled as m and n , is expected to be uncorrelated. It takes the form as [54]

$$C_{mn} = \delta_{mn} \sigma_n^2. \quad (4.4)$$

Here, the measurement error σ_n is comprised of foreground residuals and thermal noise of instruments in the n -th frequency band. It can be represented as

$$\sigma_n^2 = T_{\text{sky}}^2(\nu_n) \left(\frac{\epsilon_0^2 \theta_{\text{fg}}^2}{4\pi f_{\text{sky}}} + \frac{1}{t_{\text{int}} B} \right), \quad (4.5)$$

in which the first term at the right hand side stands for the foreground residuals while the second term denotes the thermal noise of instruments.

Substituting eqs. (4.2) to (4.5) into eq. (4.1), we obtain a specific form of Fisher information matrix for the Hongmeng mission, i.e., [53–55]

$$F_{ij} = \sum_{n=1}^{N_{\text{ch}}} \left[2 + \left(\frac{\epsilon_0^2 \theta_{\text{fg}}^2}{4\pi f_{\text{sky}}} + \frac{1}{t_{\text{int}} B} \right)^{-1} \right] \frac{d \log T_{\text{sky}}(\nu_n)}{dp_i} \frac{d \log T_{\text{sky}}(\nu_n)}{dp_j}. \quad (4.6)$$

Here, ϵ_0 represents the fraction of foreground residuals in the foreground, and θ_{fg} is the angular resolution of the foreground model, which is fixed as 5° [55]. The parameter f_{sky} denotes the sky-coverage fraction, which is fixed as 0.8. In addition, t_{int} and B , respectively, represent the integration time and bandwidth. The signal is divided into N_{ch} frequency bands, with each corresponding to a redshift bin. The information of frequency bands is listed in Table 2 of Ref. [47]. We consider several integration durations ranging from 600 seconds to 1000 hours, and the bandwidth is taken to be 1 MHz. In Fig. 1, we show the measurement errors of the Hongmeng mission for three integration durations.

The model considered in our present work is determined by a set of independent parameters, i.e.,

$$\mathbf{p} = \{t_\star, a_\star, a_{\text{esc}}, \log_{10} f_\star, \log_{10} f_{\text{esc}}, \log_{10} L_X, \langle \sigma v \rangle \text{ or } \tau^{-1} \text{ or } f_{\text{PBH}}\}. \quad (4.7)$$

The former six parameters correspond to the astrophysical parameters, for which we follow the conventions of 21cmFAST [52]. In specific terms, the parameters in question are defined as follows: t_\star represents a characteristic dimensionless star formation time scale, a_\star signifies the exponent of a power-law stellar-to-halo mass ratio function, a_{esc} denotes the exponent of a power-law escape fraction function of stellar-emitted UV photons, $\log_{10} f_\star$ denotes the logarithmic coefficient of a power-law stellar-to-halo mass ratio function, $\log_{10} f_{\text{esc}}$ stands for the logarithmic coefficient of the exponent of the power-law escape fraction function of stellar-emitted UV photons, and $\log_{10} L_X$ represents the logarithmic X-ray luminosity per unit star formation rate. The unit of L_X is $\text{erg} \cdot \text{yr} \cdot \text{sec}^{-1} M_\odot^{-1}$, where M_\odot stands for the solar mass. The last set of parameters is associated with DM, where $\langle \sigma v \rangle$ characterizes the annihilation of DM particles, τ^{-1} represents the decay of DM particles, and f_{PBH} signifies the abundance of PBHs. For the fiducial model in Fig. 1, the astrophysical parameters are assumed to be $t_\star = 0.5$, $a_\star = 0.5$, $a_{\text{esc}} = -0.5$, $\log_{10} f_\star = -1.3$, $\log_{10} f_{\text{esc}} = -1.0$, and $\log_{10} L_X = 40.0$, while the other parameters, namely f_{PBH} , $\langle \sigma v \rangle$, and τ^{-1} vanished.

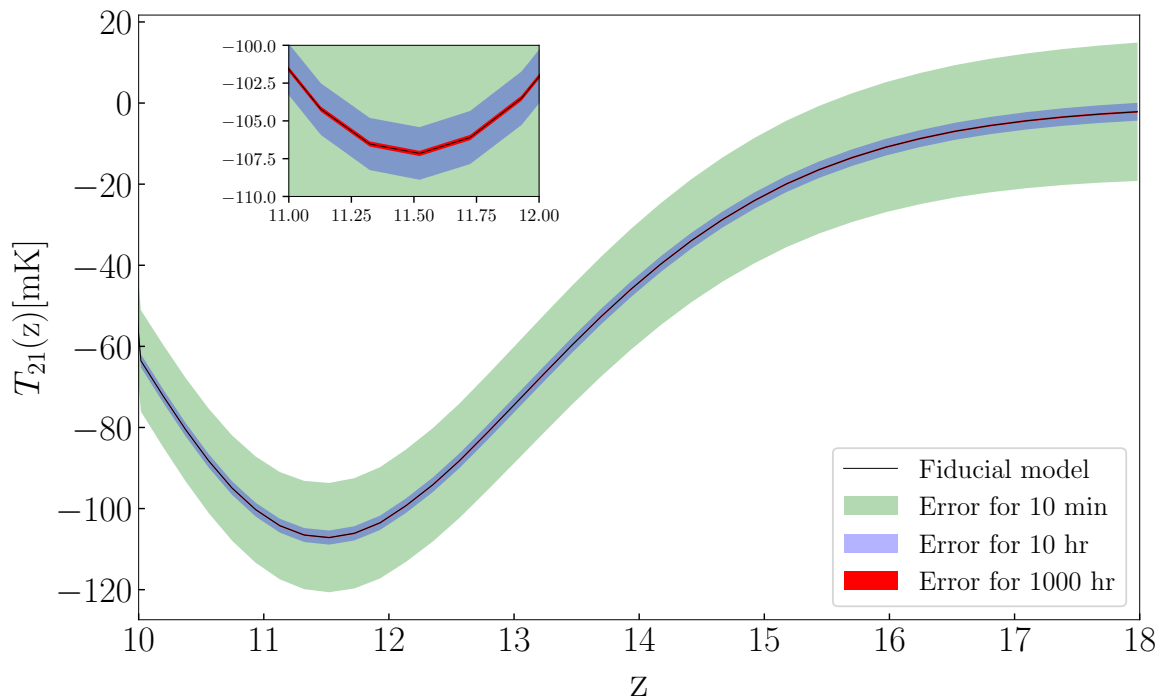


Figure 1. Measurement errors of the Hongmeng mission for three integration durations, as demonstrated by shaded regions. The fiducial model of the 21 cm global signal is shown as a black curve.

5 Hongmeng’s discovering potential

In this section, we demonstrate results of the prospective sensitivity of the Hongmeng mission to search for DM. We also compare the capability of the Hongmeng mission with those of other experiments.

5.1 Results for DM particles

We show the results of Fisher-matrix analysis in Fig. 2 (annihilation) and Fig. 3 (decay). In each figure, the left panels show triangle plots to show correlations and constraints imposed on the model parameters for three interaction channels by considering the mass of DM particles $m_\chi = 100$ MeV and $m_\chi = 100$ GeV, and integration duration of 1000 hours. The dark and light shaded regions, respectively, stand for two-dimensional contours at 1σ and 2σ confidence levels, while the solid curves represent for one-dimensional marginalized posterior probability distribution functions. Here, we let the fiducial model to be the same as that of Fig. 1. For the same channels, the right panels show the prospective 1σ -confidence-level sensitivity of the Hongmeng mission to search for the annihilation or decay of DM particles in the mass range of $10^6 - 10^{12}$ eV by considering several different foreground residuals and integration durations. For comparison, we further depict the existing upper limits at 2σ confidence level from observations of the CMB distortions (Planck 2018 results, gray solid curves) [57], gamma rays (Fermi-LAT, High Energy Stereoscopic System (H.E.S.S), Very Energetic Radiation Imaging Telescope Array System (VERITAS), Major Atmospheric Gamma

Imaging Cherenkov telescopes (MAGIC)) [14, 58–63], and electron-positron pairs (Voyager-1, black curve) [64, 65].

The analysis of the left panels in Fig. 2 and Fig. 3 reveals subtle correlations between the annihilation or decay parameters of DM particles and the astrophysical parameters. This suggests a limited degeneracy between the exotic energy injection from the annihilation and decay of DM and the astrophysical processes affecting the 21 cm global signal. Consequently, it is feasible to simultaneously determine the annihilation or decay parameters of DM particles and the astrophysical parameters. In essence, this enables the extraction of characteristic information about DM particles, such as their thermally-averaged annihilation cross-section $\langle\sigma v\rangle$ and lifetime τ .

The analysis of right panels of Fig. 2 reveal that the Hongmeng mission demonstrates greater sensitivity in detecting DM particles through the annihilation channel $\chi\chi \rightarrow e^+e^-$ compared to other channels like $\chi\chi \rightarrow \gamma\gamma$ and $\chi\chi \rightarrow b\bar{b}$. Focusing on the optimal annihilation channel $\chi\chi \rightarrow e^+e^-$, depicted in the upper right panel of Fig. 2, our results indicate that enhancing sensitivity is achievable by reducing foreground residuals, as evidenced by the comparison of the purple and blue solid curves. Additionally, extending integration durations, as seen in the comparison of the blue solid, dashed, and dot-dashed curves, also leads to a significant improvement in sensitivity for the Hongmeng mission. Ultimately, the sensitivity of the Hongmeng mission can be notably enhanced through either minimizing foreground residuals or prolonging integration durations.

Analyzing the upper right panel of Fig. 2, we can further evaluate the potential sensitivity of the Hongmeng mission by comparing it with the aforementioned upper limits on $\langle\sigma v\rangle$. With a foreground residual of approximately $\epsilon \sim 10^{-4}$ and an integration duration of 1000 hours, as indicated by the red curve, the sensitivity of the Hongmeng mission appears to be in line with the most stringent constraints represented by the gray solid curves. This suggests that the Hongmeng mission is poised to test existing results in the near future. Referring to eq. (4.5), we find that for the red curve, a foreground residual of $\epsilon_0 = 10^{-4}$ and thermal noise over an integration duration of 16.7 hours contribute equally to the measurement error of the Hongmeng mission. Consequently, the dominant factor affecting the measurement error for the red curve is the foreground residual rather than thermal noise. By reducing the foreground residuals, the sensitivity of the Hongmeng mission can be further improved. This improvement is illustrated by the blue dot-dashed curve, which showcases a negligible foreground residual with an equivalent integration duration to the red curve. Additionally, it is anticipated that the Hongmeng mission, compared to existing experiments, can explore the annihilation of lighter DM particles, particularly in the sub-GeV mass regimes.

Based on the right panels in Fig. 3, we find that the Hongmeng mission is more sensitive to search for DM particles through the decay channel $\chi \rightarrow e^+e^-$ than other annihilation channels $\chi \rightarrow \gamma\gamma$ and $\chi \rightarrow b\bar{b}$. For the sake of illustration, we focus on analysis of the optimal decay channel, i.e., $\chi \rightarrow e^+e^-$, for which our results are shown in the right upper panel in Fig. 3. We find the influence of foreground residuals and integration durations on the prospective sensitivity of the Hongmeng mission to search for the decay of DM particles. On the one hand, suppressing the foreground residuals, we can significantly enhance the sensitivity of the Hongmeng mission for an integration duration of 600 seconds. This result can be demonstrated by the purple, red, and blue solid curves, which correspond to $\epsilon_0 = 10^{-1}$, 10^{-3} , and 0, respectively. Therefore, for upcoming observations and data analysis, it is important to develop efficient methods of foreground subtractions. On the other hand, increasing the integration durations, we can also significantly suppress the thermal noise of the

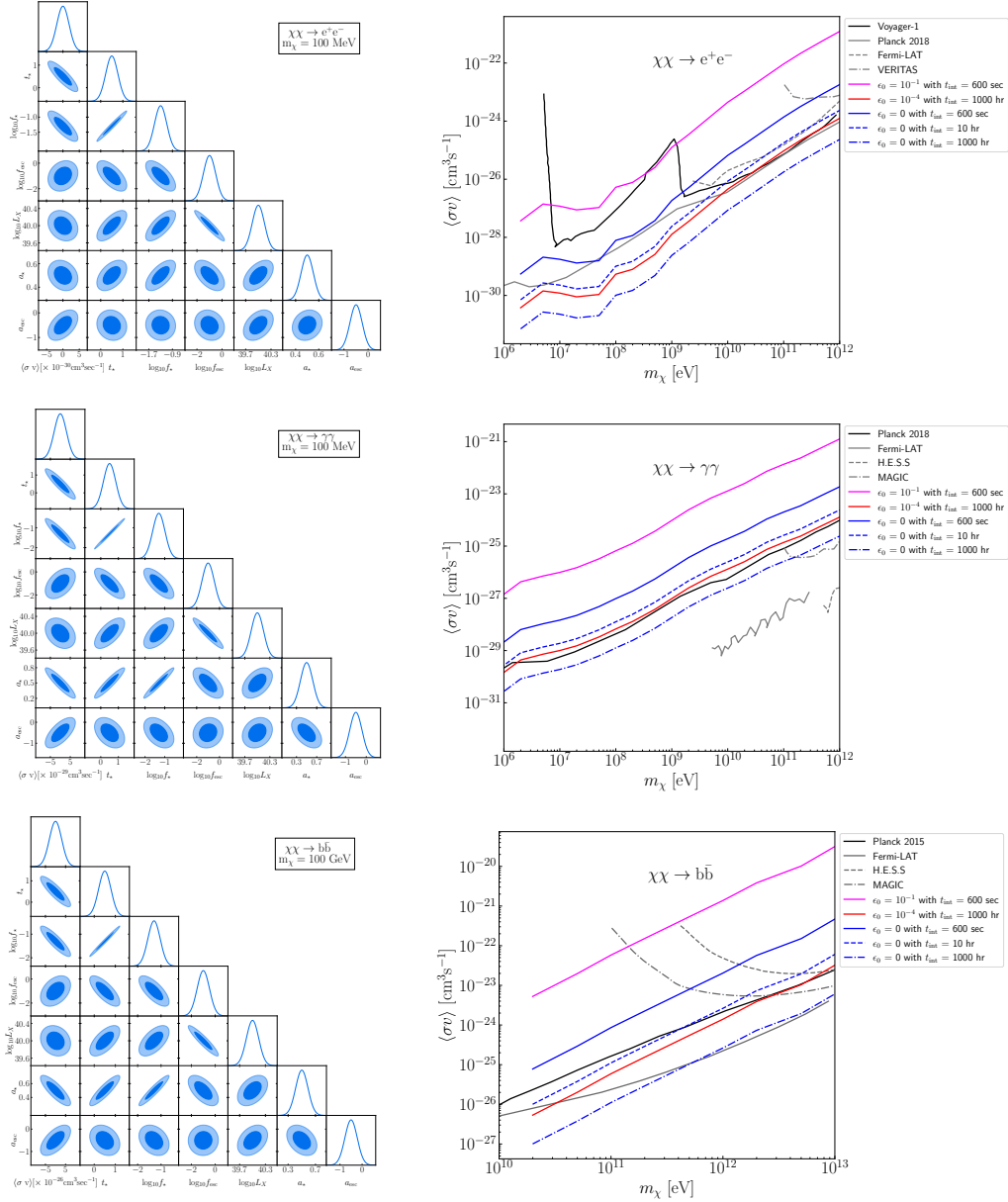


Figure 2. Prospective sensitivity of the Hongmeng mission for searching the annihilation of DM particles. Left panels: Triangle plots of the model parameters are depicted. Dark and light shaded regions correspond to contours at 1σ and 2σ confidence levels, respectively. Solid curves represent the marginalized posteriors of the model parameters. Fiducial model used is consistent with that shown in Fig. 1. For demonstration, masses of DM particles are assumed to be $m_\chi = 100$ MeV and $m_\chi = 100$ GeV, with an integration duration of 1000 hours. Right panels: Right panels illustrate the 1σ -confidence-level sensitivity of the Hongmeng mission (purple, red, and blue curves) to measure the thermally-averaged annihilation cross-section of DM particles within the mass range of $10^6 - 10^{12}$ eV. Additionally, existing upper limits at 2σ confidence level from observations of CMB distortion (Planck 2018 results, gray solid curve) [57], gamma-ray observations (H.E.S.S, VERITAS, MAGIC, and Fermi Large Area Telescope (Fermi-LAT), gray dashed and dot-dashed curves) [14, 58–63], and electron-positron pairs (Voyager-1, black curve) [66, 67] are included for comparison.

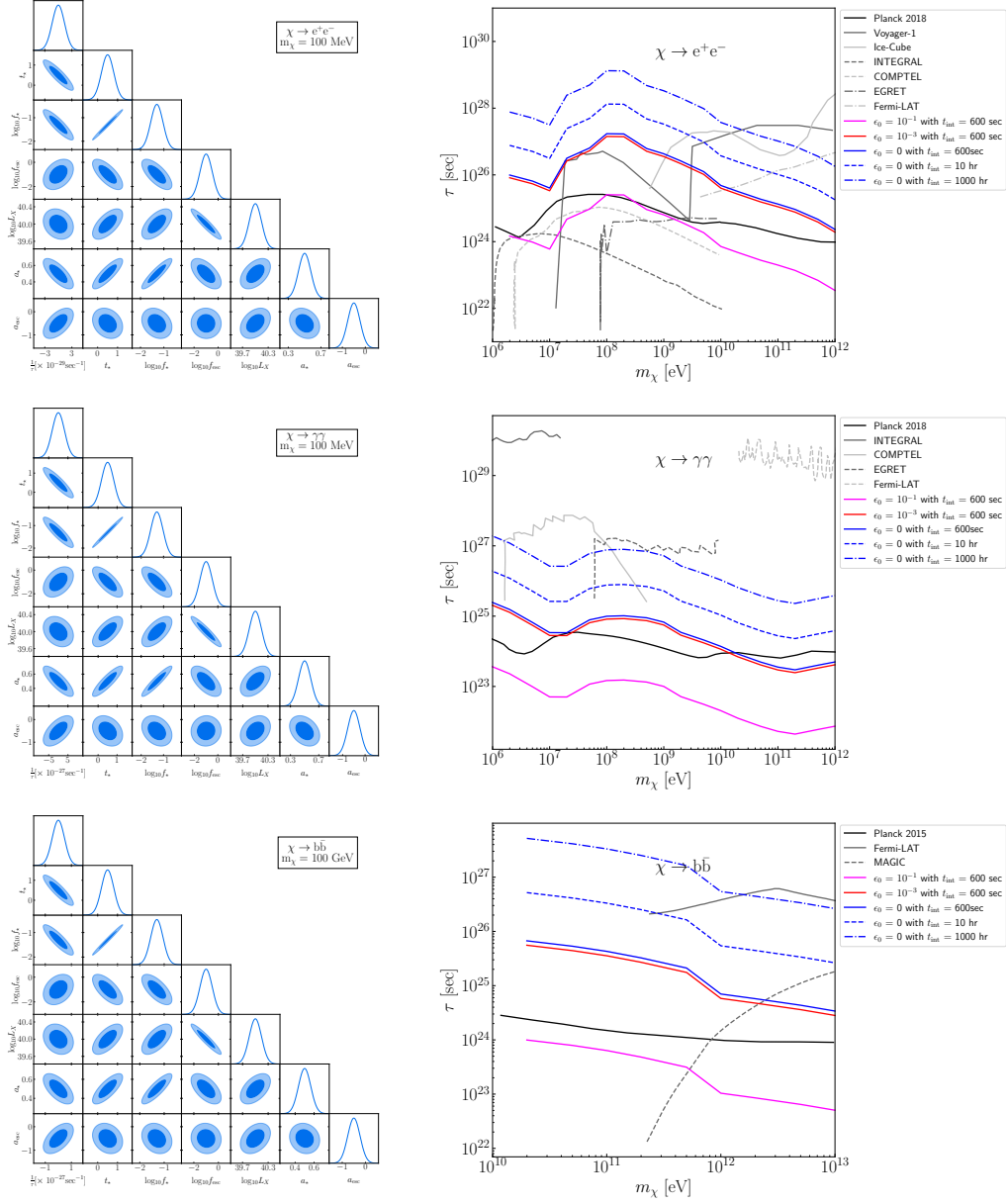


Figure 3. Prospective sensitivity of the Hongmeng mission for searching the decay of DM particles. Left panels: Triangle plots of model parameters show contours at 1σ and 2σ confidence levels, with solid curves indicating marginalized posteriors. The assumed DM particle mass are $m_\chi = 100$ MeV and $m_\chi = 100$ GeV, integrated over 1000 hours, consistent with the fiducial model in Fig. 1. Right panels: Right panels demonstrate the 1σ -confidence-level sensitivity of the Hongmeng mission (purple, red, and blue curves) in measuring the annihilation cross-section of DM particles within the mass range of $10^6 - 10^{12}$ eV. Existing upper limits at 2σ confidence level from observations of CMB distortion (Planck 2018 results, black curve) [38, 39, 68], extragalactic photons (Ice-Cube, INTEGRAL, COMPTEL, EGRET, Fermi-LAT, gray dashed and dot-dashed curves) [58, 66, 69–74], and electron-positron pairs (Voyager-1, gray solid curve) [66, 66, 67] are included for comparison.

Hongmeng instrument and thereby enhance its sensitivity. This result can be demonstrated by the blue solid, dashed, and dot-dashed curves, which correspond to $t_{\text{int}} = 600$ seconds, 10 hours, and 1000 hours, respectively. Therefore, in order to effectively search for the decay of DM particles, it is also important to get a longer observation duration. In summary, the sensitivity can be significantly enhanced via either suppressing the foreground residuals or increasing the integration durations.

Comparing the red and blue solid curves in the upper right panel of Fig. 3, we can see that the foreground residual with $\epsilon_0 = 10^{-3}$ and the thermal noise for an integration duration of 600 seconds contribute equally to the measurement error of the Hongmeng mission. When $\epsilon_0 \gg 10^{-3}$, for example, $\epsilon_0 = 10^{-2}$, the foreground residual becomes the dominant factor affecting the measurement error. In such cases, increasing the integration duration would not effectively improve the sensitivity of the Hongmeng mission. On the other hand, if we manage to reduce the foreground to $\epsilon_0 \lesssim 10^{-3}$, the thermal noise would then play a more significant role in the measurement error. Therefore, extending the integration duration to $t_{\text{int}} \gtrsim 600$ seconds could substantially enhance the sensitivity of the Hongmeng mission, as the relationship $\sigma_n \propto t_{\text{int}}^{-1/2}$ from eq. (4.5) indicates.

As shown in the right upper panel in Fig. 3, we can compare the prospective sensitivity of the Hongmeng mission with the aforementioned upper limits on τ . When considering a foreground residual of $\epsilon_0 \sim 10^{-3}$ and integration duration of 600 seconds, we find that the sensitivity of the Hongmeng mission can be comparable with the tightest ones, denoted as the black curve and gray solid curve, indicating that the existing results can be tested by the Hongmeng mission in the near future. When considering lower foreground residuals and longer integration durations, we show that the sensitivity of the Hongmeng mission can be further enhanced, as mentioned above. This can be illustrated by the blue solid curve, which corresponds to a vanishing foreground residual and the same integration duration as the red curve. In addition, we expect that compared with the existing experiments, the Hongmeng mission can search for the decay of less-massive DM particles, particularly in the sub-GeV mass regimes.

5.2 Results for PBHs

We summarize the results of Fisher-matrix analysis in Fig. 4. In the left panel, we depict the triangle plots to show correlations and constraints imposed on the model parameters by considering the PBHs of mass 10^{16} g and integration duration of 1000 hours. To be specific, the dark and light shaded regions, respectively, stand for two-dimensional contours at 1σ and 2σ confidence levels, while the solid curves represent for one-dimensional marginalized posterior probability distribution functions. Here, we let the fiducial model to be the same as that of Fig. 1. In the right panel, we show the prospective 1σ -confidence-level sensitivity of the Hongmeng mission to search for the Hawking radiation of PBHs in the mass range of $10^{15} - 10^{18}$ g by considering several different foreground residuals and integration durations. For comparison, we further depict the existing upper limits at 2σ confidence level from observations of the diffusion neutrino background (Super-Kamionkande, black curve) [75, 76], CMB anisotropies (Planck 2018 results, gray solid curve) [77–80], extra-galactic photons (a combination of the High Energy Astrophysical Observatory (HEAO), the Imaging Compton Telescope (COMPTEL), the Energetic Gamma-ray Experiment Telescope (EGRET), and the Fermi Large Area Telescope (Fermi-LAT), gray dashed curve) [77, 81], and electron-positron pairs (Voyager-1, green curve) [66, 67].

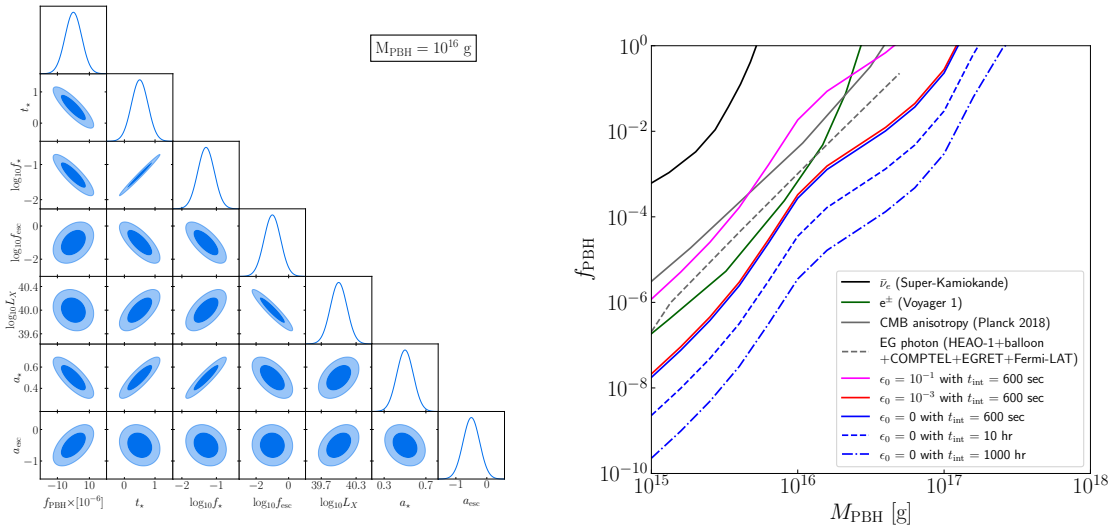


Figure 4. Prospective sensitivity of the Hongmeng mission for searching the Hawking radiation of PBHs. Left panel: Triangle plots of the model parameters. The dark and light shaded regions, respectively, represent contours at 1σ and 2σ confidence levels, while the solid curves stand for marginalized posteriors of model parameters. The fiducial model is the same as that of Fig. 1. For illustration, we consider the mass of PBHs of $M_{\text{PBH}} = 10^{16} \text{ g}$. We set the integration duration to be 1000 hours. Right panel: The 1σ -confidence-level sensitivity of the Hongmeng mission (purple, red, and blue curves) to measure the abundance of PBHs in the mass range of $10^{15} - 10^{18} \text{ g}$. For comparison, we show the existing upper limits at 2σ confidence level from observations of the diffusion neutrino background (Super-Kamiokande, black curve) [75, 76], CMB anisotropies (Planck 2018 results, gray solid curve) [78–80], extra-galactic photons (HEAO, COMPTEL, EGRET, and Fermi-LAT, gray dashed curve) [77, 81], and electron-positron pairs (Voyager-1, green curve) [66, 67].

Based on the left panel, we find that there are slight correlations between the parameter f_{PBH} and the astrophysical parameters. This result indicates little degeneracy between the exotic energy injection due to the Hawking radiation of PBHs and the astrophysical processes that influence the 21 cm global signal. Therefore, we can simultaneously measure f_{PBH} and the astrophysical parameters. In other words, we could extract the information of PBHs such as their mass function in principle.

Based on the right panel, we find the influence of foreground residuals and integration durations on the prospective sensitivity of the Hongmeng mission to search for PBHs. On the one hand, suppressing the foreground residuals, we can significantly enhance the sensitivity of the Hongmeng mission for an integration duration of 600 seconds. This result can be demonstrated by the purple, red, and blue solid curves, which correspond to $\epsilon_0 = 10^{-1}$, 10^{-3} , and 0, respectively. Therefore, for upcoming observations and data analysis, it is important to develop efficient methods of foreground subtractions. On the other hand, increasing the integration durations, we can also significantly suppress the thermal noise of the Hongmeng instrument and thereby enhance its sensitivity. This result can be demonstrated by the blue solid, dashed, and dot-dashed curves, which correspond to $t_{\text{int}} = 600$ seconds, 10 hours, and 1000 hours, respectively. Therefore, in order to effectively search for PBHs and their Hawking radiation, it is also important to get a longer observation duration.

Comparing the red and blue solid curves in the right panel, we find that the foreground residual with $\epsilon_0 = 10^{-3}$ and the thermal noise for the integration duration 600 seconds can

contribute equally to the measurement error of the Hongmeng mission. When considering $\epsilon_0 \gg 10^{-3}$, e.g., $\epsilon_0 = 10^{-2}$, the foreground residual would dominate the measurement error. In this case, increasing the integration duration would ineffectively improve the sensitivity of the Hongmeng mission. In contrast, if we could effectively subtract the foreground such that $\epsilon_0 \lesssim 10^{-3}$, the thermal noise would dominate the measurement error. Therefore, increasing the integration duration, i.e., $t_{\text{int}} \gtrsim 600$ seconds, can significantly enhance the sensitivity of the Hongmeng mission, since we now have approximately a relation of $\sigma_n \propto t_{\text{int}}^{-1/2}$ according to eq. (4.5).

We can compare our results with the existing upper limits from astronomical observations, as shown in Fig. 4. When considering a foreground residual of $\epsilon_0 \sim 10^{-2}$ and integration duration of 600 seconds, we find that the sensitivity of the Hongmeng mission can be comparable with the tightest ones, denoted as the green curve and gray dashed curve, indicating that the existing results can be tested by the Hongmeng mission in the near future. When considering lower foreground residuals and longer integration durations, we show that the sensitivity of the Hongmeng mission can be further enhanced, as mentioned above. For example, the Hongmeng mission can be sensitive to $f_{\text{PBH}} \simeq 10^{-9}$ for PBHs of mass 10^{15} g and an integration duration of 10 hours and a vanishing foreground residual. In addition, we expect that compared the existing experiments, the Hongmeng mission can search for more-massive PBHs, particularly in the mass range around 10^{17} g that otherwise can not be explored.

6 Summary

This study has explored the potential sensitivity of the Hongmeng mission in detecting the annihilation, decay of DM particles, and the Hawking radiation from PBHs by observing the 21 cm global spectrum. It is anticipated that these processes would introduce exotic energy into the IGM, leading to changes in the 21 cm global signal during cosmic dawn. By employing Fisher-matrix analysis, we have evaluated the expected sensitivity of the Hongmeng mission to the relevant model parameters, offering valuable insights for future experimental planning and data analysis. Our findings indicate that the Hongmeng mission is well-positioned to detect DM particles and PBHs in the near future.

The Hongmeng mission has the potential to detect the annihilation of DM particles, specifically focusing on the channel that produces positron-electron pairs, which offers the highest sensitivity for detection. However, in order for the Hongmeng mission to reach sensitivity levels comparable to current astronomical observational constraints, it would need to address challenges such as foreground residuals of around 10^{-4} and integration times of approximately 10^3 hours. Failure to meet these requirements could impede the mission's ability to achieve its objectives. Therefore, significant technical challenges must be overcome in the future to ensure successful detection in this regard.

The Hongmeng mission is capable of observing the decay of DM particles, particularly focusing on the decay channel that results in positron-electron pairs, offering superior detection sensitivity. To achieve sensitivity levels comparable to current astronomical observational limits, the mission would need to address challenges such as foreground residuals of approximately 10^{-3} and an integration duration of 600 seconds. Enhancing sensitivity practically could be achieved by extending the integration duration. Therefore, through the examination of the 21 cm global signal, the Hongmeng mission shows potential for detecting the decay of DM particles within the sub-GeV mass range, surpassing current observational

limits in detection sensitivity. However, the implementation of effective foreground subtraction methods remains crucial for the success of these detection efforts.

On the other hand, the search for Hawking radiation from PBHs is relatively more straightforward for the Hongmeng mission. To achieve sensitivity levels comparable to current astronomical observational limits, the mission would need to address challenges such as foreground residuals of around 10^{-2} and an integration duration of 600 seconds. Practical enhancements in sensitivity could be achieved by extending the integration duration. In comparison to existing astronomical experiments, the Hongmeng mission has the ability to detect more massive PBHs, a feat that proves challenging for other experiments.

Given the stringent requirements for foreground subtraction in DM detection, it is crucial to emphasize the importance and urgent need for the development of effective foreground subtraction methods, such as artificial intelligence [82]. However, the specifics of this research will be left for future consideration.

Acknowledgments

S.W. and X.Z. would like to express their gratitude to Xian Gao and Jiarui Sun for their warm hospitality during the final stage of this work, which was conducted during a visit to the Sun Yat-sen University. We are grateful to Kazunori Kohri and Xukun Zhang for their valuable contributions to the discussion. This work is supported by the National SKA Program of China (Grant Nos. 2022SKA0110200, 2022SKA0110203, 2023YFC2206403) and the National Natural Science Foundation of China (Grant Nos. 12473001, 12175243, and 11975072).

References

- [1] PARTICLE DATA GROUP collaboration, *Review of particle physics*, *Phys. Rev. D* **110** (2024) 030001.
- [2] K. Bechtol et al., *Dark Matter Science in the Era of LSST*, [1903.04425](#).
- [3] M. Schumann, *Direct Detection of WIMP Dark Matter: Concepts and Status*, *J. Phys. G* **46** (2019) 103003 [[1903.03026](#)].
- [4] G. Bertone and D. Hooper, *History of dark matter*, *Rev. Mod. Phys.* **90** (2018) 045002 [[1605.04909](#)].
- [5] J.M. Gaskins, *A review of indirect searches for particle dark matter*, *Contemp. Phys.* **57** (2016) 496 [[1604.00014](#)].
- [6] J.L. Feng, *Dark Matter Candidates from Particle Physics and Methods of Detection*, *Ann. Rev. Astron. Astrophys.* **48** (2010) 495 [[1003.0904](#)].
- [7] G. Bertone, D. Hooper and J. Silk, *Particle dark matter: Evidence, candidates and constraints*, *Phys. Rept.* **405** (2005) 279 [[hep-ph/0404175](#)].
- [8] V. Sahni, *Dark matter and dark energy*, *Lect. Notes Phys.* **653** (2004) 141 [[astro-ph/0403324](#)].
- [9] P.F. Smith and J.D. Lewin, *Dark Matter Detection*, *Phys. Rept.* **187** (1990) 203.
- [10] T. Lin, *Dark matter models and direct detection*, *PoS* **333** (2019) 009 [[1904.07915](#)].
- [11] FERMI-LAT, DES collaboration, *Searching for Dark Matter Annihilation in Recently Discovered Milky Way Satellites with Fermi-LAT*, *Astrophys. J.* **834** (2017) 110 [[1611.03184](#)].

- [12] MAGIC, FERMI-LAT collaboration, *Limits to Dark Matter Annihilation Cross-Section from a Combined Analysis of MAGIC and Fermi-LAT Observations of Dwarf Satellite Galaxies*, *JCAP* **02** (2016) 039 [[1601.06590](#)].
- [13] T.R. Slatyer and C.-L. Wu, *General Constraints on Dark Matter Decay from the Cosmic Microwave Background*, *Phys. Rev. D* **95** (2017) 023010 [[1610.06933](#)].
- [14] FERMI-LAT collaboration, *Searching for Dark Matter Annihilation from Milky Way Dwarf Spheroidal Galaxies with Six Years of Fermi Large Area Telescope Data*, *Phys. Rev. Lett.* **115** (2015) 231301 [[1503.02641](#)].
- [15] T.R. Slatyer, *Indirect dark matter signatures in the cosmic dark ages. I. Generalizing the bound on s-wave dark matter annihilation from Planck results*, *Phys. Rev. D* **93** (2016) 023527 [[1506.03811](#)].
- [16] H.E.S.S. collaboration, *Search for Photon-Linelike Signatures from Dark Matter Annihilations with H.E.S.S.*, *Phys. Rev. Lett.* **110** (2013) 041301 [[1301.1173](#)].
- [17] G. Steigman, B. Dasgupta and J.F. Beacom, *Precise Relic WIMP Abundance and its Impact on Searches for Dark Matter Annihilation*, *Phys. Rev. D* **86** (2012) 023506 [[1204.3622](#)].
- [18] X.-L. Chen and M. Kamionkowski, *Particle decays during the cosmic dark ages*, *Phys. Rev. D* **70** (2004) 043502 [[astro-ph/0310473](#)].
- [19] P. Gondolo and J. Silk, *Dark matter annihilation at the galactic center*, *Phys. Rev. Lett.* **83** (1999) 1719 [[astro-ph/9906391](#)].
- [20] S. Hawking, *Gravitationally collapsed objects of very low mass*, *Mon. Not. Roy. Astron. Soc.* **152** (1971) 75.
- [21] M. Sasaki, T. Suyama, T. Tanaka and S. Yokoyama, *Primordial black holes—perspectives in gravitational wave astronomy*, *Class. Quant. Grav.* **35** (2018) 063001 [[1801.05235](#)].
- [22] B. Carr, K. Kohri, Y. Sendouda and J. Yokoyama, *Constraints on primordial black holes*, *Rept. Prog. Phys.* **84** (2021) 116902 [[2002.12778](#)].
- [23] A.M. Green and B.J. Kavanagh, *Primordial Black Holes as a dark matter candidate*, *J. Phys. G* **48** (2021) 043001 [[2007.10722](#)].
- [24] B. Carr and F. Kuhnel, *Primordial black holes as dark matter candidates*, *SciPost Phys. Lect. Notes* **48** (2022) 1 [[2110.02821](#)].
- [25] J. Auffinger, *Primordial black holes as dark matter and Hawking radiation constraints with BlackHawk*, Ph.D. thesis, Institut de Physique des 2 Infinis de Lyon, France, IP2I, Lyon, 2022.
- [26] Y. Sun, J.W. Foster, H. Liu, J.B. Muñoz and T.R. Slatyer, *Inhomogeneous Energy Injection in the 21-cm Power Spectrum: Sensitivity to Dark Matter Decay*, [2312.11608](#).
- [27] H. Liu, W. Qin, G.W. Ridgway and T.R. Slatyer, *Exotic energy injection in the early Universe. I. A novel treatment for low-energy electrons and photons*, *Phys. Rev. D* **108** (2023) 043530 [[2303.07366](#)].
- [28] H. Liu and T.R. Slatyer, *Implications of a 21-cm signal for dark matter annihilation and decay*, *Phys. Rev. D* **98** (2018) 023501 [[1803.09739](#)].
- [29] H. Liu, W. Qin, G.W. Ridgway and T.R. Slatyer, *Exotic energy injection in the early Universe. II. CMB spectral distortions and constraints on light dark matter*, *Phys. Rev. D* **108** (2023) 043531 [[2303.07370](#)].
- [30] C. Xu, W. Qin and T.R. Slatyer, *CMB limits on decaying dark matter beyond the ionization threshold*, *Phys. Rev. D* **110** (2024) 123529 [[2408.13305](#)].
- [31] F. Capozzi, R.Z. Ferreira, L. Lopez-Honorez and O. Mena, *CMB and Lyman- α constraints on dark matter decays to photons*, in *Beyond Standard Model: From Theory to Experiment*, 2024, DOI.

- [32] H. Liu, W. Qin, G.W. Ridgway and T.R. Slatyer, *Lyman- α constraints on cosmic heating from dark matter annihilation and decay*, *Phys. Rev. D* **104** (2021) 043514 [2008.01084].
- [33] J.D. Bowman, A.E.E. Rogers, R.A. Monsalve, T.J. Mozdzen and N. Mahesh, *An absorption profile centred at 78 megahertz in the sky-averaged spectrum*, *Nature* **555** (2018) 67 [1810.05912].
- [34] A.K. Saha and R. Laha, *Sensitivities on nonspinning and spinning primordial black hole dark matter with global 21-cm troughs*, *Phys. Rev. D* **105** (2022) 103026 [2112.10794].
- [35] J. Cang, Y. Gao and Y.-Z. Ma, *21-cm constraints on spinning primordial black holes*, *JCAP* **03** (2022) 012 [2108.13256].
- [36] H.T.J. Bevins, A. Fialkov, E.d.L. Acedo, W.J. Handley, S. Singh, R. Subrahmanyam et al., *Astrophysical constraints from the SARAS 3 non-detection of the cosmic dawn sky-averaged 21-cm signal*, *Nature Astron.* **6** (2022) 1473 [2212.00464].
- [37] X. Chen, J. Yan, Y. Xu, L. Deng, F. Wu, L. Wu et al., *Discovering the Sky at the Longest Wavelength Mission - A Pathfinder for Exploring the Cosmic Dark Ages.*, *Chinese Journal of Space Science* **43** (2023) 43.
- [38] PLANCK collaboration, *Planck 2018 results. VI. Cosmological parameters*, *Astron. Astrophys.* **641** (2020) A6 [1807.06209].
- [39] T.R. Slatyer, *Indirect Dark Matter Signatures in the Cosmic Dark Ages II. Ionization, Heating and Photon Production from Arbitrary Energy Injections*, *Phys. Rev. D* **93** (2016) 023521 [1506.03812].
- [40] M. Cirelli, G. Corcella, A. Hektor, G. Hutsi, M. Kadastik, P. Panci et al., *PPPC 4 DM ID: A Poor Particle Physicist Cookbook for Dark Matter Indirect Detection*, *JCAP* **03** (2011) 051 [1012.4515].
- [41] C. Bierlich et al., *A comprehensive guide to the physics and usage of PYTHIA 8.3*, *SciPost Phys. Codeb.* **2022** (2022) 8 [2203.11601].
- [42] T.R. Slatyer, *Energy Injection And Absorption In The Cosmic Dark Ages*, *Phys. Rev. D* **87** (2013) 123513 [1211.0283].
- [43] T.R. Slatyer, N. Padmanabhan and D.P. Finkbeiner, *CMB Constraints on WIMP Annihilation: Energy Absorption During the Recombination Epoch*, *Phys. Rev. D* **80** (2009) 043526 [0906.1197].
- [44] H. Liu, G.W. Ridgway and T.R. Slatyer, *Code package for calculating modified cosmic ionization and thermal histories with dark matter and other exotic energy injections*, *Phys. Rev. D* **101** (2020) 023530 [1904.09296].
- [45] R. Takahashi and K. Kohri, *Cosmological boost factor for dark matter annihilation at redshifts of $z=10-100$ using the power spectrum approach*, *Phys. Rev. D* **104** (2021) 103518 [2107.00897].
- [46] J. Auffinger and A. Arbey, *BlackHawk: A tool for computing Black Hole evaporation*, *PoS TOOLS2020* (2021) 024 [2012.12902].
- [47] G. Facchinetti, L. Lopez-Honorez, Y. Qin and A. Mesinger, *21cm signal sensitivity to dark matter decay*, *JCAP* **01** (2024) 005 [2308.16656].
- [48] O. Mena, S. Palomares-Ruiz, P. Villanueva-Domingo and S.J. Witte, *Constraining the primordial black hole abundance with 21-cm cosmology*, *Phys. Rev. D* **100** (2019) 043540 [1906.07735].
- [49] V. Poulin, P.D. Serpico, F. Calore, S. Clesse and K. Kohri, *CMB bounds on disk-accreting massive primordial black holes*, *Phys. Rev. D* **96** (2017) 083524 [1707.04206].
- [50] S. Furlanetto, S.P. Oh and F. Briggs, *Cosmology at Low Frequencies: The 21 cm Transition and the High-Redshift Universe*, *Phys. Rept.* **433** (2006) 181 [astro-ph/0608032].

- [51] J.R. Pritchard and A. Loeb, *21-cm cosmology*, *Rept. Prog. Phys.* **75** (2012) 086901 [[1109.6012](#)].
- [52] A. Mesinger, S. Furlanetto and R. Cen, *21cmFAST: A Fast, Semi-Numerical Simulation of the High-Redshift 21-cm Signal*, *Mon. Not. Roy. Astron. Soc.* **411** (2011) 955 [[1003.3878](#)].
- [53] M. Tegmark, A. Taylor and A. Heavens, *Karhunen-Loeve eigenvalue problems in cosmology: How should we tackle large data sets?*, *Astrophys. J.* **480** (1997) 22 [[astro-ph/9603021](#)].
- [54] J.R. Pritchard and A. Loeb, *Constraining the unexplored period between the dark ages and reionization with observations of the global 21 cm signal*, *Phys. Rev. D* **82** (2010) 023006 [[1005.4057](#)].
- [55] X.-W. Liu, C. Heneka and L. Amendola, *Constraining coupled quintessence with the 21cm signal*, *JCAP* **05** (2020) 038 [[1910.02763](#)].
- [56] S. Jester and H. Falcke, *Science with a lunar low-frequency array: from the dark ages of the Universe to nearby exoplanets*, *New Astron. Rev.* **53** (2009) 1 [[0902.0493](#)].
- [57] Z.-X. Zhang, Y.-M. Wang, J. Cang, Z. Zhang, Y. Liu, S.-Y. Li et al., *Dark matter search with CMB: a study of foregrounds*, *JCAP* **10** (2023) 002 [[2304.07793](#)].
- [58] M. Cirelli, N. Fornengo, B.J. Kavanagh and E. Pinetti, *Integral X-ray constraints on sub-GeV Dark Matter*, *Phys. Rev. D* **103** (2021) 063022 [[2007.11493](#)].
- [59] HESS collaboration, *Searches for gamma-ray lines and 'pure WIMP' spectra from Dark Matter annihilations in dwarf galaxies with H.E.S.S.*, *JCAP* **11** (2018) 037 [[1810.00995](#)].
- [60] H.E.S.S. collaboration, *Search for dark matter annihilation signatures in H.E.S.S. observations of Dwarf Spheroidal Galaxies*, *Phys. Rev. D* **90** (2014) 112012 [[1410.2589](#)].
- [61] VERITAS collaboration, *Dark Matter Constraints from a Joint Analysis of Dwarf Spheroidal Galaxy Observations with VERITAS*, *Phys. Rev. D* **95** (2017) 082001 [[1703.04937](#)].
- [62] MAGIC collaboration, *Indirect dark matter searches in the dwarf satellite galaxy Ursa Major II with the MAGIC Telescopes*, *JCAP* **03** (2018) 009 [[1712.03095](#)].
- [63] J. Aleksić et al., *Optimized dark matter searches in deep observations of Segue 1 with MAGIC*, *JCAP* **02** (2014) 008 [[1312.1535](#)].
- [64] M. Boudaud, J. Lavalle and P. Salati, *Novel cosmic-ray electron and positron constraints on MeV dark matter particles*, *Phys. Rev. Lett.* **119** (2017) 021103 [[1612.07698](#)].
- [65] M. Boudaud, T. Lacroix, M. Stref and J. Lavalle, *Robust cosmic-ray constraints on p-wave annihilating MeV dark matter*, *Phys. Rev. D* **99** (2019) 061302 [[1810.01680](#)].
- [66] T. Cohen, K. Murase, N.L. Rodd, B.R. Safdi and Y. Soreq, *γ -ray Constraints on Decaying Dark Matter and Implications for IceCube*, *Phys. Rev. Lett.* **119** (2017) 021102 [[1612.05638](#)].
- [67] M. Boudaud and M. Cirelli, *Voyager 1 e^\pm Further Constrain Primordial Black Holes as Dark Matter*, *Phys. Rev. Lett.* **122** (2019) 041104 [[1807.03075](#)].
- [68] F. Capozzi, R.Z. Ferreira, L. Lopez-Honorez and O. Mena, *CMB and Lyman- α constraints on dark matter decays to photons*, *JCAP* **06** (2023) 060 [[2303.07426](#)].
- [69] R. Essig, E. Kuflik, S.D. McDermott, T. Volansky and K.M. Zurek, *Constraining Light Dark Matter with Diffuse X-Ray and Gamma-Ray Observations*, *JHEP* **11** (2013) 193 [[1309.4091](#)].
- [70] A. Massari, E. Izaguirre, R. Essig, A. Albert, E. Bloom and G.A. Gómez-Vargas, *Strong Optimized Conservative Fermi-LAT Constraints on Dark Matter Models from the Inclusive Photon Spectrum*, *Phys. Rev. D* **91** (2015) 083539 [[1503.07169](#)].
- [71] D. Cadamuro and J. Redondo, *Cosmological bounds on pseudo Nambu-Goldstone bosons*, *JCAP* **02** (2012) 032 [[1110.2895](#)].
- [72] J. Koechler, *X-rays constraints on sub-GeV Dark Matter*, in *TeV Particle Astrophysics 2023*, 9, 2023 [[2309.10043](#)].

- [73] F. Calore, A. Dekker, P.D. Serpico and T. Siegert, *Constraints on light decaying dark matter candidates from 16 yr of INTEGRAL/SPI observations*, *Mon. Not. Roy. Astron. Soc.* **520** (2023) 4167 [2209.06299].
- [74] J.W. Foster, Y. Park, B.R. Safdi, Y. Soreq and W.L. Xu, *Search for dark matter lines at the Galactic Center with 14 years of Fermi data*, *Phys. Rev. D* **107** (2023) 103047 [2212.07435].
- [75] V. Poulin, J. Lesgourgues and P.D. Serpico, *Cosmological constraints on exotic injection of electromagnetic energy*, *JCAP* **03** (2017) 043 [1610.10051].
- [76] S. Wang, D.-M. Xia, X. Zhang, S. Zhou and Z. Chang, *Constraining primordial black holes as dark matter at JUNO*, *Phys. Rev. D* **103** (2021) 043010 [2010.16053].
- [77] B.J. Carr, K. Kohri, Y. Sendouda and J. Yokoyama, *Constraints on primordial black holes from the Galactic gamma-ray background*, *Phys. Rev. D* **94** (2016) 044029 [1604.05349].
- [78] J. Chluba, A. Ravenni and S.K. Acharya, *Thermalization of large energy release in the early Universe*, *Mon. Not. Roy. Astron. Soc.* **498** (2020) 959 [2005.11325].
- [79] S.K. Acharya and R. Khatri, *CMB and BBN constraints on evaporating primordial black holes revisited*, *JCAP* **06** (2020) 018 [2002.00898].
- [80] S. Clark, B. Dutta, Y. Gao, L.E. Strigari and S. Watson, *Planck Constraint on Relic Primordial Black Holes*, *Phys. Rev. D* **95** (2017) 083006 [1612.07738].
- [81] B.J. Carr, K. Kohri, Y. Sendouda and J. Yokoyama, *New cosmological constraints on primordial black holes*, *Phys. Rev. D* **81** (2010) 104019 [0912.5297].
- [82] A. Tripathi, A. Datta, M. Choudhury and S. Majumdar, *Extracting the Global 21-cm signal from Cosmic Dawn and Epoch of Reionization in the presence of Foreground and Ionosphere*, *Mon. Not. Roy. Astron. Soc.* **528** (2024) 1945 [2401.01935].